

Wills Aligner: A Robust Multi-Subject Brain Representation Learner

Guangyin Bao¹, Zixuan Gong¹, Qi Zhang¹, Jialei Zhou¹,
Wei Fan², Kun Yi³, Usman Naseem⁴, Liang Hu¹, Duoqian Miao¹

1 Tongji University 2 University of Oxford 3 Beijing Institute of Technology 4 Macquarie University
zhangqi_cs@tongji.edu.cn

ABSTRACT

Decoding visual information from human brain activity has seen remarkable advancements in recent research. However, due to the significant variability in cortical parcellation and cognition patterns across subjects, current approaches personalized deep models for each subject, constraining the practicality of this technology in real-world contexts. To tackle the challenges, we introduce *Wills Aligner*, a robust multi-subject brain representation learner. Our *Wills Aligner* initially aligns different subjects' brains at the anatomical level. Subsequently, it incorporates a mixture of brain experts to learn individual cognition patterns. Additionally, it decouples the multi-subject learning task into a two-stage training, propelling the deep model and its plugin network to learn inter-subject commonality knowledge and various cognition patterns, respectively. *Wills Aligner* enables us to overcome anatomical differences and to efficiently leverage a single model for multi-subject brain representation learning. We meticulously evaluate the performance of our approach across coarse-grained and fine-grained visual decoding tasks. The experimental results demonstrate that our *Wills Aligner* achieves state-of-the-art performance.

CCS CONCEPTS

• **Computing methodologies** → **Artificial intelligence**; • **Applied computing** → *Computational biology*; • **Human-centered computing** → *Human computer interaction (HCI)*.

KEYWORDS

Neuroscience, fMRI, Multi-Subject, Representation Learning, Brain Visual Decoding, Few-shot Learning

1 INTRODUCTION

The process of human perception is marvelous. Our perception of things is not only determined by the objective real world but also closely related to individual subjective will. Understanding human perceptual processes is a key step in deciphering the complex mechanisms of the brain, facilitating the development of brain-inspired computational models [7, 27, 29, 31], and having a wide range of applications in clinical medicine [22] and brain-computer interfaces [18, 26]. Within this broad research field, visual decoding is an important and challenging branch that allows us to explore the complex mechanisms of the human brain during visual processing, object recognition, and scene understanding [30, 47]. Among the various modalities of the brain, functional magnetic resonance imaging (fMRI) has been widely used by researchers due to its non-invasive acquisition and easy localization of the functional cortex. This paper focuses on visual decoding based on fMRI.

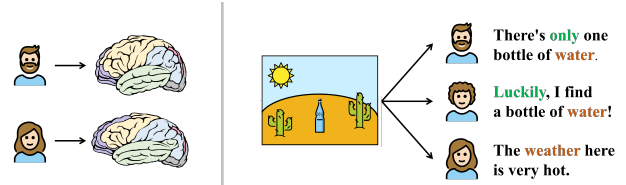


Figure 1: Illustrations of inter-subject brain differences. The left figure illustrates anatomical differences, with subjects having different sizes and locations of the same functional areas (marked in the same color). The right figure shows differences in cognition patterns, where different subjects perceive the same thing differently.

Previous works [15, 20, 23, 28, 36, 37] have investigated representation learning in brain visual decoding tasks. They construct classification and retrieval tasks to mine visual information from fMRI. However, existing methods face significant limitations in their practical application since they are customized for individuals, i.e., a subject-specific deep model is trained using the subject's own fMRI, leading to a consistent increase in the number of models required, which is attributed to the presence of individually significant brain differences. To this end, there is a pressing need to investigate and develop multi-subject visual decoding models. As shown in Figure 1, brain differences are reflected in anatomical and cognition pattern differences due to the diversity of genetics and cognition formation processes. Anatomical differences refer to differences in cortical parcellation among subjects. The size and location of each functional area, such as the visual, language, and memory areas, vary and can only be pinpointed through anatomical structures like the gray and white matter of the brain [6, 11]. Cognition pattern differences refer to the fact that subjects feel, think, and understand things differently due to variances in individual focus, historical experience, and prior knowledge.

Currently, there has been limited exploration of multi-subject visual decoding, and the performance achieved is often inferior to that of single-subject models. Some approaches [4, 48] address anatomical differences by employing conventional data processing such as PCA downscaling or padding, resulting in brain information loss and misalignment of functional regions. Other methods [10] achieve fMRI alignment by training linear models using the same images seen by different subjects, while this approach is challenging to generalize to a large number of subjects due to the requirement of identical visual stimuli. Fortunately, advancements in neuroscience research allow us to address the challenge of anatomical differences by registering each fMRI with a standardized brain template based

on prior knowledge of the brain’s anatomical structure. However, when it comes to addressing cognition pattern differences, existing methods either directly extend single-subject models to handle multi-subject fMRI or employ subject-specific tokens to identify each subject [3, 48]. Despite a decent effort, these strategies do not enhance the model’s fitting capacity, resulting in poor generalization to each subject and subpar performance. Furthermore, we recognize that multi-subject learning necessitates simultaneous mastery of inter-subject common visual knowledge and different cognition patterns. This requirement introduces trade-offs during model training, limits the transfer of inter-subject knowledge, and leads to inconsistent optimization directions. For these issues, it is suggested to add specific learnable parameters for each cognition pattern to enhance the model’s fit capacity and decouple multi-subject learning into two independent optimization stages.

In light of the above discussion, we introduce **Wills Aligner** in this paper. We first use a well-established fMRI registration technique to eliminate anatomical differences, which we call anatomical alignment. To learn various cognition patterns, we introduce Mixture of Brain Experts (MoBE), a plugin network that can be added to the mainstream brain decoding model (backbone) to equip it with the ability to fit various cognition patterns. In addition, we decouple multi-subject brain representation learning into two phases: a commonality knowledge learning phase and a various cognition patterns learning phase. We harness the semantic structure of visual stimuli to steer the backbone in acquiring subject-agnostic commonality knowledge, achieving inter-subject knowledge transfer so that visual decoding of specific subjects can benefit from other subjects’ fMRI data. We identify the appropriate brain experts within the plugin network through routing selection, and then various cognition patterns are learned using corresponding brain experts.

We conducted an extensive evaluation on the Natural Scene Dataset (NSD) [1], which shows our Wills Aligner achieves state-of-the-art performance. Specifically, we obtain an 81% improvement in multi-subject coarse-grained visual decoding, while in fine-grained visual decoding, we achieve a 15% improvement compared to the single-subject method under the same settings. More experiments demonstrate the robustness and few-shot ability of our method.

Our contributions are summarized as follows:

- We use prior knowledge of the brain’s anatomical structure to overcome anatomical differences and experimentally demonstrate its effectiveness in visual decoding.
- We propose the Mixture of Brain Experts plugin network, which can enhance the backbone network in learning various cognition patterns.
- We innovatively decouple multi-subject representation learning into two phases, successfully handling trade-offs and achieving inter-subject knowledge transfer.

2 RELATED WORKS

2.1 fMRI Visual Decoding

The study of brain visual decoding using fMRI has been a long-standing endeavor [17, 25, 44]. At the model architecture level, due to the low signal-to-noise ratio of fMRI, early studies [40] emphasize the use of purely linear models, such as linear regression, to

embed fMRI and images into a common intermediate space. Further studies [7, 15, 39] use VGG networks to extract semantically rich image representations. Mind-Reader [20] uses ResNet [14] to enhance fMRI representation learning. MindEye [37] demonstrates that a large MLP can serve as an excellent brain representation learner. Other [4, 5, 48] work attempt to use the Transformer [43] architecture in brain visual decoding. In order to reduce the number of model parameters and increase the model inference speed, Lite-Mind [12] uses a frequency domain learner. At the level of the optimization objectives, early studies [15, 36] use the cross-entropy of categorization tasks as supervised objectives. Recognizing visual stimuli categories from fMRI can decode coarse-grained visual information. Mind-Reader [20] first uses an fMRI-to-image retrieval task based on the Info-NCE loss to decode fine-grained visual information. Thanks to the success of large pre-trained visual models, Brain-Diffuser [28] applies the CLIP loss [32] to align fMRI representations to the CLIP ViT’s latent space. MindEye [37] proposes the data enhancement strategy BiMixCo for fMRI and uses SoftCLIP loss to achieve high-performance fMRI visual decoding. Some other work explored self-supervised learning. MinD-Vis [4] and Mind-Video [5] use Masked Brain Modeling for pre-training. Due to the large variation among subjects, the above methods almost train proprietary single-subject models for each subject. CLIP-MUSED [48] first studies multi-subject brain representation learning and visual decoding, but its performance barely reaches the level of a single-subject model.

2.2 Multi-Subject fMRI Alignment

How to align fMRIs of different subjects to address cortical size diversity is key to group analysis. In neuroscience, anatomical alignment [11] denotes the process of comparing and matching neuroanatomical structures across various individuals. This is achieved by assessing the shape of the cerebral cortex and the distribution patterns of gray and white matter, serving as pivotal reference points. Previous works [10, 13] have argued that anatomical alignment would lose information and thus fail to meet the demands of visual decoding, so they preferred to use functional alignment. FUGW [41] learns the voxel transformation matrix using optimal transmission from source to target subjects. CLIP-MUSED [48] uses principal component analysis to project voxels from each cortical region to the same dimension. In MinD-Vis [4], fMRI data are padded to the maximum length in a wrap-around manner.

2.3 Mixture of Experts

The mixture of experts (MoE) [19, 38] is a machine learning model that combines several expert models from different domains for better performance and generalization capabilities. The core idea of MoE is to utilize the strengths of different expert models to address the limitations and challenges a single model faces. With a routing model, MoE adaptively assigns weights to individual experts.

MoE has numerous applications in computer vision [35, 45, 49], natural language processing [8, 9], and multimodal learning [2, 46], where it can improve model training efficiency and performance. Inspired by this, we intend to modify neural networks in a similar way to learn various cognition patterns.

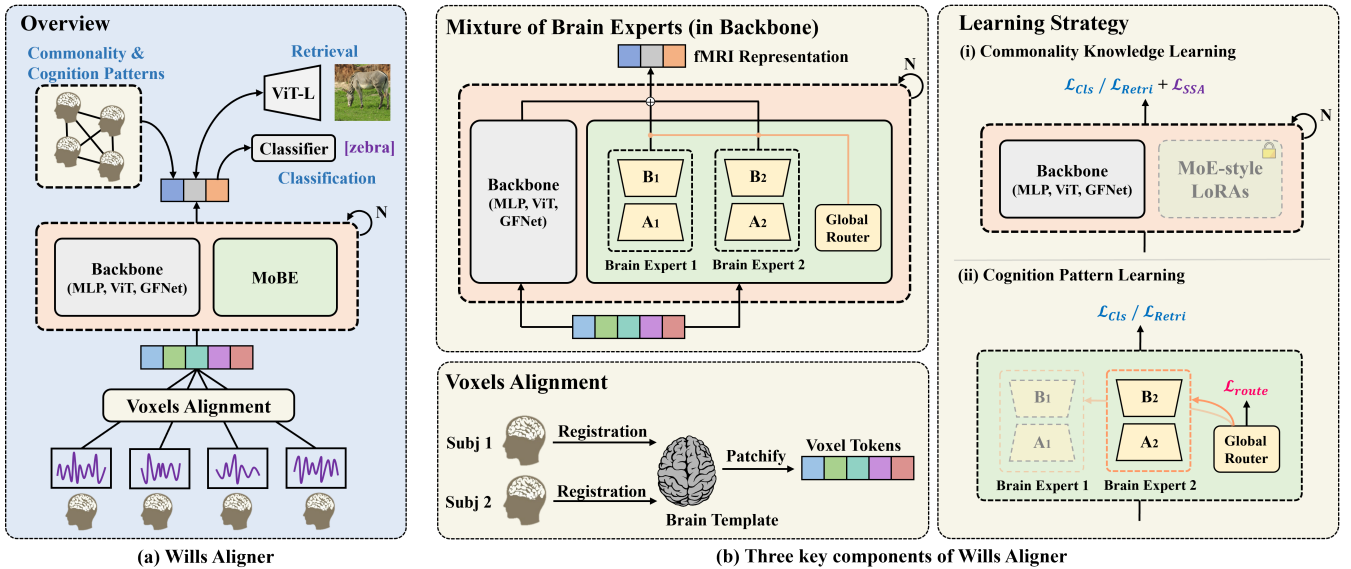


Figure 2: Overview of our Wills Aligner. Figure (a) illustrates the overall flowchart of our method. Figure (b) shows its three key components: Voxel Alignment, MoBE, and Learning Strategy, corresponding to Section 3.2 through 3.4 in turn.

2.4 Low-Rank Adapters

The Low-Rank Adapter (LoRA) [16] is a method for parameter-efficient fine-tuning. It can reduce memory requirements by using a small set of trainable parameters, while not updating the original model parameters which remain fixed. During fine-tuning, the gradients generated by the optimizer are passed through the fixed model to the LoRA. Subsequently, the LoRA can update its own parameters to fit the optimization objective.

3 METHOD

3.1 Overview

As illustrated in Figure 2, our **Wills Aligner** comprises three key components: 1) **Voxels Alignment**, an fMRI preprocessing, which aligns fMRI voxels from different subjects at the anatomical level, using a standardized brain template. 2) **Mixture of Brain Experts**, a plugin network for cognition pattern learning, which consists of multiple brain experts and a global router. 3) **Learning Strategy**, a two-stage training to learn inter-subject commonality knowledge and various cognition patterns.

3.2 Voxels Alignment

The anatomical differences among individuals lead to inter-subject inconsistency in voxel counts and voxel correspondence. To enable deep learning models to embed fMRI data from multiple subjects uniformly, we need to perform voxel alignment so that the voxels are the same length and the cortical areas correspond one to the other. In contrast to the functional alignment commonly adopted in Section 2.2, we use anatomical alignment. This is due to the fact that the anatomical alignment technique enables voxel alignment on high-resolution brain maps and does not depend on any learnable parameters and training. We believe in the validity of

anatomical alignment as we are inspired by the computer vision area, where image scaling does not affect the deep model’s learning of its semantics.

Anatomical Alignment for fMRI. Anatomical alignment relies on fMRI registration techniques, a well-established mapping that delineates a unique correspondence between each location in one brain and its counterpart in another. Specifically, we map the fMRI data from different subjects to a standard brain template. The brain template utilized in our study is *fsaverage7*, a triangular surface mesh created via the spherical registration of 40 individuals using an energy minimization algorithm to align surface-based features [11]. FreeSurfer provides registration tools facilitating the alignment of any brain to this brain template. Following anatomical alignment, the fMRI data pertaining to specific cortical areas across all subjects is converted into one-dimensional voxel sequences.

Patchify and Tokenization. Sampling an fMRI from the dataset, we utilize X to denote the voxel sequence after registering to the *fsaverage7* brain template. we firstly divide X into n non-overlapping patches $X = [X_1, X_2, \dots, X_n]$. Each patch contains an equal number of voxels, and we use zero padding to fill the last patch. Then, we adopt 1-D convolutions with positional encoding to obtain multiple tokens.

$$T = [T_1, T_2, \dots, T_n] = Conv(X) + PE. \quad (1)$$

Thus, we have completed Voxels Alignment. Depending on the specific model architecture, the aligned voxels X or tokens T will serve as inputs of the neural network model.

3.3 Mixture of Brain Experts

In this section, we will describe the design of our Mixture of Brain Experts (MoBE). MoBE functions as a plugin network, integrating

multiple brain cognition pattern experts. Each brain expert is assigned weights through a global router. Along with the backbone, MoBE will be deployed into each linear layer of the neural network.

Brain Cognition Pattern Experts. Formally, for a traditional linear layer parameterized by weight W_0 and bias b , its transform operation o can be denoted as:

$$o = W_0x + b, \quad (2)$$

where $x \in \mathbb{R}^d$ represents the input tensor. We integrate multiple brain experts into this linear layer to accommodate multi-subject learning tasks. Specifically, assuming that multi-subject fMRI data contains k cognition patterns, we implement k brain experts. Those brain experts, parameterized by ΔW_i , $i = 1, 2, \dots, k$, maintain a parallel relationship with the original linear layer parameters W_0 . Consequently, the forward process of each linear layer with MoBE can be represented as:

$$o = (W_0 + \sum_{i=1}^k \omega_i \Delta W_i)x + b, \quad (3)$$

where ω_i represents the weight coefficient assigned to each brain expert, which is determined by a router.

Global Router. A network (backbone) contains multiple linear layers. Thus, multiple MoBEs are employed. In the traditional MoE, each expert is controlled by its own proprietary router. These routers are parameterized by tiny neural networks. However, in some task scenarios, such as our multi-subject learning, it is necessary for the behavior of all MoEs to remain consistent. Therefore, adopting proprietary routers can cause severe parameter redundancy. Consequently, we introduce a global router. The parameterized global router is denoted by $G(\cdot)$, receiving x as input and outputting a probability distribution of length k :

$$\omega = [\omega_1, \omega_2, \dots, \omega_k] = G(x). \quad (4)$$

This probability distribution serves as the routing weight coefficient for all MoBEs in our backbone network.

Low-Rank Decomposition. Performing a low-rank decomposition on each brain expert can significantly reduce the trainable parameter count, which has been demonstrated in [16]. We denote the decomposition as:

$$\Delta W = BA, \quad (5)$$

where $A \in \mathbb{R}^{r \times d}$ and $B \in \mathbb{R}^{d \times r}$ are two low-rank matrices, with a rank of r . Moreover, random initialization is implemented for A , and zero initialization is implemented for B , enabling the initial output of each brain expert to be zero. This allows the initial output of MoBEs without any perturbation to the backbone.

Overall, the Mixture of Brain Experts is a lightweight and efficient plugin that we deploy into all linear layers of the backbone network. Under the control of the global router, the forward process of each linear layer with MoBE can be summarized as follows:

$$o = (W_0 + \sum_{i=1}^k G(X)_i B_i A_i)x + b. \quad (6)$$

3.4 Learning Strategy

This section introduces the downstream tasks and our two-stage learning strategy. Considering that the potential conflict between commonality knowledge and individual cognition patterns will

lead to a tradeoff in multi-subject learning, we decouple it into two independent learning stages.

We use $F(\cdot)$ to represent the backbone network configured with MoBEs. Sampling a sample (X, y, l, s) from the training dataset, X denotes the voxel sequence (For Transformer, replace it using voxel tokens T), y denotes the CLIP representation of corresponding visual stimuli, l denotes the category of visual stimuli, and s denotes the subject ID in the form of one-hot tensor. Based on this, the representation of fMRI can be denoted as $f = F(X)$.

3.4.1 Downstream Task Learning. Our Wills Aligner supports two mainstream tasks: classification and cross-modal retrieval. Each task uses the corresponding task loss.

Classification Task. The classification task requires classifying fMRI signals according to visual stimuli categories. We adopt the cross-entropy loss function, i.e. $CE(\cdot)$, as its supervision objective:

$$\mathcal{L}_{task} = \mathcal{L}_{cls} = CE(H(f), l), \quad (7)$$

where $H(\cdot)$ represents a classifier head mapping fMRI representation to logits.

Cross-Modal Retrieval Task. The retrieval task requires establishing a correspondence between fMRI signal and visual stimuli. It requires us to find the best matching visual stimuli for each fMRI representation and to find the most matching fMRI signal for each visual stimuli.

The optimization objective for cross-modal retrieval is to maximize the similarity between the fMRI representation and the corresponding visual stimuli representation, and we use CLIP loss as the supervision. CLIP loss consists of two unidirectional contrastive losses:

$$\mathcal{L}_{brain} = -\frac{1}{|\mathcal{B}|} \sum_{j=1}^{|\mathcal{B}|} \log \frac{\exp(f_j^\top \cdot y_j / \tau)}{\sum_{m=1}^{|\mathcal{B}|} \exp(f_j^\top \cdot y_m / \tau)}, \quad (8)$$

$$\mathcal{L}_{image} = -\frac{1}{|\mathcal{B}|} \sum_{j=1}^{|\mathcal{B}|} \log \frac{\exp(y_j^\top \cdot f_j / \tau)}{\sum_{m=1}^{|\mathcal{B}|} \exp(y_j^\top \cdot f_m / \tau)}, \quad (9)$$

where \mathcal{B} denotes a mini-batch, and τ denotes a temperature factor. On this basis, the objective can be expressed as:

$$\mathcal{L}_{task} = \mathcal{L}_{retri} = \mathcal{L}_{brain} + \mathcal{L}_{image}. \quad (10)$$

3.4.2 Multi-Subject commonality knowledge Learning. We encourage the backbone of the neural network, i.e., the original linear layers parameterized by W_0 and b , to learn multi-subject commonality knowledge.

Commonality Knowledge. Commonality knowledge is irrelevant to the subjects. We aim to make the backbone outputs of different subjects similar when they receive the same visual stimuli. However, experiments in neuroscience cannot guarantee that subjects receive the same visual stimuli. Therefore, we utilize the structural relationships of CLIP’s image representations to guide the learning of subject-agnostic fMRI representations.

Semantic Structure Alignment. We denote the fMRI representations, CLIP’s image representations, and subject IDs in a mini-batch by \mathbb{F} , \mathbb{Y} , and \mathbb{S} , respectively. Then, we construct their respective semantic structures: $\mathcal{M}_f = \mathbb{F}^\top \mathbb{F}$, $\mathcal{M}_y = \mathbb{Y}^\top \mathbb{Y}$, and $\mathcal{M}_s = \mathbb{S}^\top \mathbb{S}$. We push the fMRI representation structure close to the CLIP’s image representations and away from the subject relation structure

by Semantic Structure Alignment (SSA) loss:

$$\mathcal{L}_{SSA} = -\log \frac{\text{sim}(\mathcal{M}_f, \mathcal{M}_y)}{\text{sim}(\mathcal{M}_f, \mathcal{M}_y) + \text{sim}(\mathcal{M}_f, \mathcal{M}_s)}, \quad (11)$$

where $\text{sim}(\cdot)$ denotes the cosine similarity.

We define the overall backbone loss $\mathcal{L}_{backbone}$ network with task loss \mathcal{L}_{task} and SSA loss \mathcal{L}_{SSA} :

$$\mathcal{L}_{backbone} = \mathcal{L}_{task} + \alpha \mathcal{L}_{SSA}, \quad (12)$$

where α is the factor to balance two losses.

3.4.3 Cognition Pattern Learning. We push MoBEs to learn various cognition patterns.

Cognition Patterns. The individual cognition pattern leads to a subject-specific departure from commonality knowledge. We strive to refine the fMRI representations to deviate from the backbone outputs, enhancing individuality and distinctiveness.

Routing Selection. Since the number of cognition patterns will not exceed the subject count, we set the cognition pattern count k equal to the number of subjects. Each cognitive pattern is represented by a proprietary forward process route. We determine the correspondence between each fMRI and cognition pattern through routing selection. Subsequently, we use subject classification tasks to optimize the global router via the cross-entropy loss:

$$\mathcal{L}_{route} = CE(\omega, s). \quad (13)$$

Based on this, brain experts corresponding to specific cognition patterns, i.e., all brain experts in the proprietary route, are optimized under the supervision of task loss \mathcal{L}_{task} . Combined with some prior neuroscience knowledge, we can manually set the cognition pattern counts by clustering similar subjects.

4 EXPERIMENT

4.1 Dataset

The Natural Scenes Dataset (NSD) is a massive 7T neuroscience dataset encompassing fMRI data from 8 subjects. Throughout the NSD experiment, participants were presented with images sourced from MSCOCO [21], while their neural responses were recorded utilizing a high-resolution 7-Tesla fMRI scanner. Our study aligns with previous research by concentrating on Subj01, Subj02, Subj05, and Subj07, as these 4 subjects completed all 40 session scans. Within the dataset, each subject’s train set comprises 8859 distinct visual stimuli and 24980 fMRI, wherein each image was repetitively presented for viewing 1-3 times. The test set contains 982 visual stimuli and 2770 fMRI. It is crucial to emphasize that within the training set for each subject, the visual stimuli employed do not overlap with those utilized for other subjects. However, the same visual stimuli are employed across subjects within the test set. Upon selecting the cortical area named *nsdgeneral*, we acquired voxel sequences for the four subjects, whose lengths are 15724, 14278, 13039, and 12682, respectively.

Then, we conduct our **Voxel Alignment**. The voxel sequences from distinct subjects are registered to the *fsaverage7* brain template. It standardizes voxel sequences from *nsdgeneral* with a uniform voxel count of 37984. Subsequently, we employ a 1-D convolution with an 1187 convolution kernel size and an 1187 stride for patchifying the sequences, thereby generating 32 voxel tokens.

4.2 Model Architectures

We use three different backbone networks to evaluate the robustness of our Wills Aligners. The hyperparameter r in MoBEs is designated as 16. Table 1 displays the number of parameters for the backbone and MoBEs. More details can be found in Appendix A.

MLP. We use an MLP backbone containing 4 ResBlocks to embed the voxel sequence X . **For the classification task**, the fMRI representation has a dimension of 768, which is subsequently mapped to a probability distribution of 80 classes by a classification head. **For the retrieval task**, the fMRI representation has a dimension of 257×768 , the same as the image CLIP representation. Then, we use a retrieval projector that applies a dimension-preserving transformation for fMRI representation.

Transformer. We use a 6-layer standard Transformer to embed the 32 voxel tokens T together with a CLS token. The fMRI representation has a dimension of 33×768 . **For the classification task**, the input of the classification head is the CLS token obtained from fMRI representation. **For the retrieval task**, we extend each non-CLS token to $8 \times$ with a linear layer so that the final dimension of fMRI representation is 257×768 .

GFNet. Previous work [12] has shown that frequency-domain learners can effectively learn fMRI representation. Therefore, we use GFNet [33, 34] as our backbone network, which replaces the self-attention layers with frequency domain filters. **For the downstream tasks**, we use settings similar to Transformer.

Model Architecture	Number of Parameters	
	Backbone	MoBEs
MLP Classification	226.0M	5.2M (2.2%)
MLP Retrieval	506.4M	17.0M (3.2%)
Transformer Classification	17.6M	1.6M (8.3%)
Transformer Retrieval	35.9M	2.5M (6.5%)
GFNet Classification	15.3M	1.8M (10.5%)
GFNet Retrieval	33.7M	2.7M (7.4%)

Table 1: Parameter counts comparison between backbone and MoBEs. Our MoBEs only bring a few additional parameters to the backbone.

4.3 Classification Experiment

The classification task stands as a coarse-grained brain visual decoding, which demands extracting and recognizing the categories of visual stimuli contained within fMRI data.

4.3.1 Experiment Settings. Baselines. We compare Wills Aligner with existing multi-subject classification methods on the NSD dataset. The Single-Subject method uses data from a single subject to train the proprietary model. The Multi-Subject method puts all the subjects’ fMRI into training together. EMB learns a token for each subject to encode their identity. CLIP-MUSED [48] is based on EMB [3] and learns high-level and low-level semantic tokens through CLIP representation similarity analysis. Note that all baselines use principal component analysis (PCA) to align fMRI, while Wills Aligner uses our voxel alignment.

Implementation Details. We use the AdamW [24] optimizer to train three backbones. The learning rate is searched in [1e-4, 3e-4, 5e-4, 1e-3, 3e-3, 5e-3] using a linear learning rate decay with

Method	Model Architecture	Number of Parameters	mAP \uparrow	AUC \uparrow	Hamming \downarrow
Single-Subject	MLP	-	0.258	0.854	0.033
Single-Subject	Transformer	66M	0.238	0.815	0.032
Multi-Subject	MLP	-	0.150	0.767	0.039
Multi-Subject	Transformer	66M	0.156	0.755	0.038
EMB [3]	Transformer	66M	0.220	0.825	0.035
CLIP-MUSED [48]	Transformer	66M	0.258	0.877	0.030
Wills Aligners (ours)	MLP	231M	0.467	0.945	0.023
Wills Aligners (ours)	Transformer	19M	0.424	0.937	0.024
Wills Aligners (ours)	GFNet	17M	0.443	0.941	0.024

Table 2: Experiment results of the multi-label classification task. All baseline results are quoted from CLIP-MUSED [48]. We report the average value of four subjects, and our results are averaged over three runs.

Method	Model and Loss	Number of Parameters	Retrieval Accuracy	
			Image (fwd) \uparrow	Brain (bwd) \uparrow
Mind Reader [20]	Deep Models + InfoNce Loss	2M	11.0%	49.0%
Brain Diffuser [28]	Linear Regression Models + CLIP Loss	3B	29.9%	21.4%
MindEye [37]	MLP + CLIP loss	996M	83.7%	79.1%
MindEye [37]	MLP + CLIP loss + MSE loss	996M	88.8%	84.9%
MindEye [37]	MLP + SoftCLIP + BiMixCo	996M	89.6%	82.2%
Wills Aligners (ours)	MLP + CLIP loss	523M	95.4%	83.9%
Wills Aligners (ours)	Transformer + CLIP loss	38M	96.6%	86.1%
Wills Aligners (ours)	GFNet + CLIP loss	36M	95.3%	81.5%

Table 3: Experiment results of the cross-modal retrieval task. All baseline results are quoted from corresponding papers, and our results are averaged over three runs. We report the results on subject 1, as previous works only give detailed results on subject 1. The results of our Wills Aligner on other subjects can be found in Appendix B.

a final learning rate of 0.01 initial value. For weight decay, we fix it to $1e-4$. We set the batch size to 2048 for the MLP and 1024 for Transformer and GFNet. For commonality knowledge learning, We set the weight of SSA loss to 0.1 and train 1000 epochs. For cognition pattern learning, we first optimize the router for 10 epochs and then optimize MoBEs for 100 epochs.

Evaluation Metrics. MSCOCO has a total of 80 categories, where each image contains multiple labels. Consistent with previous work [48], we employ three commonly used evaluation metrics in multi-label classification: mean Average Precision (mAP), the area under the receiver operating characteristic curve (AUC), and Hamming distance. Our experiment is run 3 times under different random seeds, and the averages are reported.

4.3.2 Results and Analysis. Table 2 shows the results of the classification experiment. Experimental results show that our approach achieves significant performance improvement. Our best model achieves 81% improvement in the mAP metric (0.467 v.s. 0.258), 7.8% improvement in the AUC metric (0.945 v.s. 0.877), and 23.3% improvement in Hamming distance (0.023 v.s. 0.030), indicating that our Wills Aligner achieves state-of-the-art performance in coarse-grained brain visual decoding.

Considering that both use the Transformer, Wills Aligner significantly improves classification precision, even if we have fewer parameters. Performance enhancement may stem from two perspectives. On the one hand, anatomical alignment is better than PCA. Since PCA focuses solely on the value itself without considering the brain’s prior knowledge, it tends to lose valuable information during implementation. In contrast, our voxel alignment is based

on the brain’s anatomical structure, which retains useful information to a large extent. On the other hand, our method achieves inter-subject knowledge transfer so that visual decoding for specific subjects benefits from others. The classification task requires only coarse-grained semantics; thus, commonality knowledge from other subjects is very helpful.

Comparing the three backbone networks in our approach, it’s evident they achieve similar performance levels. This underscores the robustness of our Wills Aligner, demonstrating its adaptability across diverse backbone networks. Notably, employing Transformer and GFNet leads to reduced model parameter demands compared to MLP, aligning with findings from prior research [12].

4.4 Retrieval Experiment

The brain-to-image cross-modal retrieval stands as a fine-grained brain visual decoding task, which requires fine-grained recognition of the visual semantics contained in the fMRI to be able to find the best matching image in a large retrieval pool.

4.4.1 Experiment Settings. Baselines. Since previous work on multi-subject brain representation learning has not been evaluated on the NSD cross-modal retrieval task, we compare our Wills Aligner to state-of-the-art single-subject retrieval methods. Among them, Mind-Reader [20] uses InfoNCE loss to align the fMRI representations to 768-dimensional image representations. Brain Diffuser [28] uses CLIP Loss to align the fMRI representation to the 257×768 image representation of ViT-L, using 257 separate linear regression models. MindEye [37] uses a large MLP to learn brain representations to align 257×768 image representations and uses

Few-Shot Ratio	Method	Subject 1		Subject 2		Subject 5		Subject 7	
		mAP \uparrow	AUC \uparrow						
0.05 (1 session)	Single-Subject	0.128	0.782	0.138	0.740	0.154	0.804	0.122	0.779
	Wills Aligner (ours)	0.270	0.901	0.229	0.880	0.275	0.907	0.206	0.862
0.1 (2 sessions)	Single-Subject	0.143	0.808	0.168	0.834	0.171	0.827	0.138	0.802
	Wills Aligner (ours)	0.322	0.915	0.287	0.898	0.334	0.921	0.276	0.888
0.2 (4 sessions)	Single-Subject	0.210	0.874	0.185	0.856	0.179	0.851	0.164	0.830
	Wills Aligner (ours)	0.385	0.930	0.354	0.922	0.409	0.935	0.317	0.904

Table 4: Results of few-shot classification.

Few-Shot Ratio	Method	Subject 1		Subject 2		Subject 5		Subject 7	
		Image \uparrow	Brain \uparrow						
0.05 (1 session)	Single-Subject	10.6%	1.9%	11.8%	1.2%	10.7%	1.8%	9.1%	1.2%
	Wills Aligner (ours)	65.1%	47.9%	69.9%	49.3%	47.0%	29.3%	46.3%	30.0%
0.1 (2 sessions)	Single-Subject	26.5%	4.6%	29.5%	3.5%	20.0%	3.2%	20.9%	2.6%
	Wills Aligner (ours)	75.9%	53.0%	77.4%	56.3%	53.8%	35.6%	54.8%	39.4%
0.2 (4 sessions)	Single-Subject	46.3%	13.8%	53.8%	12.8%	43.9%	8.5%	41.1%	8.6%
	Wills Aligner (ours)	82.7%	61.1%	84.2%	64.2%	64.3%	46.6%	63.0%	46.8%

Table 5: Results of few-shot retrieval.

more supervised objectives (such as MSE and SoftCLIP) and data augmentation (i.e., BiMixCo). Since we only evaluate the retrieval performance, we ignore MindEye’s reconstruction module. Note that all baselines use original voxel sequences for embedding fMRI representations while Wills Aligner conducts our voxel alignment.

Implementation Details. For all three backbones, we set the batch size to 300. We also use the AdamW optimizer with the learning rate searching in [1e-4, 3e-4, 5e-4, 1e-3, 3e-3, 5e-3, 1e-2] and the weight decay fixed at 1e-4. Both fixed and linear descent learning rates are attempted. For commonality knowledge learning, We search the weight of SSA loss in [0.5, 0.1, 0.05, 0.01] and train 300 epochs. For cognition pattern learning, we optimize the router for 10 epochs and then optimize the MoBEs for 100 epochs.

Evaluation Metrics. We evaluate model performance using Top-1 brain retrieval accuracy and Top-1 image retrieval accuracy. The calculation of the metrics follows MindEye. For image retrieval (aka forward retrieval), each test fMRI is first converted to a fMRI representation, and we compute the cosine similarity to its respective ground truth CLIP image representation and 299 other randomly selected CLIP image representations in the test set. For each test sample, success is determined if the cosine similarity is greatest between the fMRI embedding and its respective ground truth CLIP embedding (aka top-1 retrieval performance, random chance is 1/300). We repeat the evaluation for each test sample 30 times to account for the variability in the random sampling of batches. The same procedure is used for brain retrieval (aka backward retrieval), except fMRI and images are flipped. We repeat the experiment three times under different random seeds and report the average results.

4.4.2 Results and Analysis. Results of the retrieval experiment are shown in Table 3. With the same settings, all the models using our Wills Aligner outperform MindEye, achieving an almost 15.4% performance improvement in forward retrieval (96.6% v.s. 83.7%). Notably, our performance with only CLIP Loss supervision outperforms MindEye’s results with complex supervised objectives and

BiMixCo data augmentation by 7.8% (96.6% v.s. 89.6%). In addition, we used fewer model parameters (38M v.s. 996M).

We find similar performance across all three backbone models in the retrieval task. This demonstrates the robustness of our Wills Aligner. When both use MLP backbone, the result suggests that the performance enhancement provided by our method stems from inter-subject knowledge transferring rather than modification of the backbone architecture. Specifically, our Wills Aligner achieves a 14.0% performance improvement compared to MindEye (95.4% v.s. 83.7%). Since the training settings are identical and the voxel processing is equivalent, the only reason for the performance improvement could lie in the fact that our method learns the commonality knowledge required for visual decoding from other subjects and uses it to enhance the performance of Subject 1.

In addition, our method improves less on the retrieval task than the classification task, suggesting that SSA loss captures more coarse-grained categories rather than fine-grained semantics.

4.5 Few-Shot Experiment

To further explore how much a single subject’s visual decoding performance can benefit from the training data from other subjects, we conducted a few-shot visual decoding experiment. The few-shot setting is more realistic for practical applications, as collecting 40-session data for a single subject is difficult.

4.5.1 Experiment Settings. We compare our Wills Aligner with the Single-Subject Method. We employ the few-shot setting for a given subject while the other subjects use the full fMRI. Few-shot rates are set to be 0.05, 0.1, and 0.2, corresponding to 1, 2, and 4 sessions of scanned fMRI, respectively. We guarantee that the method-independent settings are identical. Specifically, we use the same backbone and voxel sequences. We set the learning rate to 1e-4 for both classification and retrieval tasks. For our approach, we upsample the few-shot subject’s fMRI to a comparable level as other subjects. The results for MLP are presented in the main text,

MoBEs	SSA	Classification			Retrieval	
		mAP \uparrow	AUC \uparrow	Hamming \downarrow	Brain \uparrow	Image \uparrow
×	×	0.314	0.904	0.027	81.6%	77.9%
✓	×	0.417	0.935	0.025	92.3%	81.4%
×	✓	0.361	0.924	0.027	85.8%	79.1%
✓	✓	0.467	0.945	0.023	95.4%	83.9%

Table 6: Ablation experiments for Wills Aligner. The results are the average of three runs.

Rank	Classification			Retrieval	
	mAP \uparrow	AUC \uparrow	Hamming \downarrow	Brain \uparrow	Image \uparrow
2	0.461	0.944	0.023	93.3%	80.5%
4	0.452	0.943	0.023	95.0%	82.4%
8	0.445	0.941	0.024	93.9%	82.6%
16	0.467	0.945	0.023	95.4%	83.9%
32	0.448	0.942	0.024	95.2%	84.7%

Table 7: Ablation experiments for rank. The results are the average of three runs.

and the corresponding results for Transformer and GFNet can be found in Appendix B.

4.5.2 Results and Analysis. Tables 4 and Table 5 show the performance of different few-shot subjects in the classification and retrieval tasks, respectively. The experimental results show that our method can significantly improve the brain visual decoding performance of few-shot subjects. In particular, for subject 1, with the same settings, we achieve a comparable forward retrieval performance to MindEye (82.7% v.s. 83.7%) while we only use 4-session fMRI (1/10 of MindEye use). This suggests that our Wills Aligner is able to transfer knowledge among subjects and assists the brain visual decoding of the few-shot subject, highlighting the importance of inter-subject commonality knowledge learning.

4.6 Ablation Experiment

We perform ablation experiments to explore the performance sources of our Wills Aligner and provide experience for the setting of MoBEs’ hyperparameter r .

Ablation for Components. We ablate two key components of our Wills Aligner. One is MoBEs together with the corresponding cognition pattern learning, and the other is the SSA loss used for learning inter-subject commonality knowledge. We conduct experiments using consistent hyperparameters and report average results under three different random seeds. The experimental results are shown in Table 6, indicating that both key components of Wills Aligner are useful for performance improvement. We also note that SSA loss does not improve performance as much as MoBE, suggesting that cognition pattern learning is more important.

Ablation for MoBEs’ Rank. A larger rank implies that the plugin introduces more additional parameters. We ablate MoBE’s rank to explore its selection. We search the rank in [2, 4, 8, 16, 32]. Experiments are conducted using fixed hyperparameters, and average results are reported for three different random seeds. We only report the results of MLP in the main text, and the results of other backbones can be found in Appendix B. As illustrated in

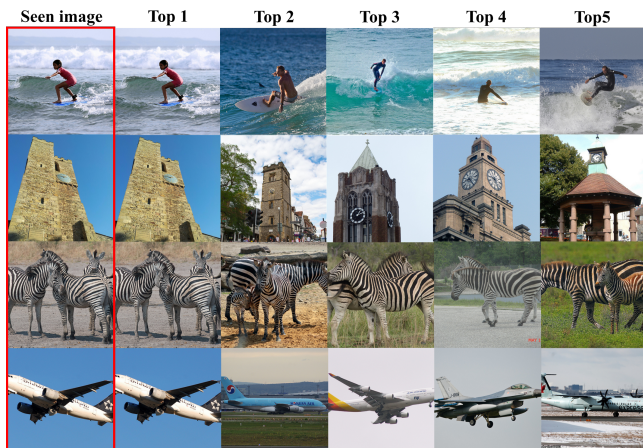


Figure 3: Examples of successful forward retrieval of Subject 1 on the entire test set.

Table 7, the best performance is achieved when the rank is chosen to be 16. However, we observe that different rank r exhibits comparable performance, indicating that our method is insensitive to this hyperparameter. This is also consistent with previous research on LoRA [16], which found that an increase in rank does not significantly improve performance.

4.7 Visualization

Figure 3 shows the visualization of our forward retrieval on the entire testing set. The results demonstrate the effectiveness of our approach in accurately retrieving visual stimuli from fMRI data. Furthermore, we observe that the top-5 retrieval outcomes consistently exhibit high semantic relevance. We have included more visualization and discussion in Appendix C, including some examples that are mismatched.

5 LIMITATION AND FUTURE WORKS

We evaluate our Wills Aligner on two brain visual decoding tasks using the NSD dataset. Whether our method generalizes to other datasets (such as GOD [15] and HCP [42]) and brain linguistic decoding tasks remains to be verified. In addition, due to the various fMRI scanners and experimental conditions, subject differences across datasets are greater than within the single dataset. Therefore, the ability to perform multi-dataset few-shot visual decoding needs to be further verified. The above challenge is also the focus of our subsequent work.

6 CONCLUSION

This paper proposes Wills Aligner, a robust multi-subject brain representation learner. It comprises voxel anatomical alignment, a mixture of brain experts, and a two-stage approach for learning commonality knowledge and various cognition patterns. We have substantiated its effectiveness and robustness through extensive experiments. We believe it holds positive implications for the field of neuroscience and multi-subject brain decoding.

REFERENCES

- [1] Emily J Allen, Ghislain St-Yves, Yihan Wu, Jesse L Breedlove, Jacob S Prince, Logan T Dowdle, Matthias Nau, Brad Caron, Franco Pestilli, Ian Charest, et al. 2022. A massive 7T fMRI dataset to bridge cognitive neuroscience and artificial intelligence. *Nature neuroscience* 25, 1 (2022), 116–126.
- [2] Hangbo Bao, Li Dong, Songhao Piao, and Furu Wei. 2022. BEiT: BERT Pre-Training of Image Transformers. In *International Conference on Learning Representations*.
- [3] Omar Chehab, Alexandre Défossez, Loiseau Jean-Christophe, Alexandre Gramfort, and Jean-Remi King. 2022. Deep Recurrent Encoder: an end-to-end network to model magnetoencephalography at scale. *Neurons, Behavior, Data analysis, and Theory* (2022).
- [4] Zijiao Chen, Jiaxin Qing, Tiange Xiang, Wan Lin Yue, and Juan Helen Zhou. 2023. Seeing Beyond the Brain: Conditional Diffusion Model with Sparse Masked Modeling for Vision Decoding. In *IEEE/CVF Conference on Computer Vision and Pattern Recognition*. IEEE, 22710–22720.
- [5] Zijiao Chen, Jiaxin Qing, and Juan Helen Zhou. 2023. Cinematic Mindscapes: High-quality Video Reconstruction from Brain Activity. In *Advances in Neural Information Processing Systems*.
- [6] Christophe Destrieux, Bruce Fischl, Anders Dale, and Eric Halgren. 2010. Automatic parcellation of human cortical gyri and sulci using standard anatomical nomenclature. *Neuroimage* 53, 1 (2010), 1–15.
- [7] Changde Du, Kaicheng Fu, Jinpeng Li, and Huiguang He. 2023. Decoding visual neural representations by multimodal learning of brain-visual-linguistic features. *IEEE Transactions on Pattern Analysis and Machine Intelligence* (2023).
- [8] Nan Du, Yanping Huang, Andrew M. Dai, Simon Tong, Dmitry Lepikhin, Yuanzhong Xu, Maxim Krikun, Yanqi Zhou, Adams Wei Yu, Orhan Firat, Barret Zoph, Liam Fedus, Maarten P. Bosma, Zongwei Zhou, Tao Wang, Yu Emma Wang, Kellie Webster, Marie Pellat, Kevin Robinson, Kathleen S. Meier-Hellstern, Toju Duke, Lucas Dixon, Kun Zhang, Quoc V. Le, Yonghui Wu, Zhifeng Chen, and Claire Cui. 2022. GLaM: Efficient Scaling of Language Models with Mixture-of-Experts. In *International Conference on Machine Learning (Proceedings of Machine Learning Research, Vol. 162)*. 5547–5569.
- [9] William Fedus, Barret Zoph, and Noam Shazeer. 2022. Switch Transformers: Scaling to Trillion Parameter Models with Simple and Efficient Sparsity. *Journal of Machine Learning Research* 23 (2022), 120:1–120:39.
- [10] Matteo Ferrante, Tommaso Boccatto, and Nicola Toschi. 2023. Through their eyes: multi-subject Brain Decoding with simple alignment techniques. *arXiv preprint arXiv:2309.06627* (2023).
- [11] Bruce Fischl, Martin I Sereno, Roger BH Tootell, and Anders M Dale. 1999. High-resolution intersubject averaging and a coordinate system for the cortical surface. *Human brain mapping* 8, 4 (1999), 272–284.
- [12] Zixuan Gong, Qi Zhang, Duoqian Miao, Guangyin Bao, and Liang Hu. 2023. Lite-Mind: Towards Efficient and Versatile Brain Representation Network. *CoRR* abs/2312.03781 (2023).
- [13] James V Haxby, J Swaroop Guntupalli, Samuel A Nastase, and Ma Feilong. 2020. Hyperalignment: Modeling shared information encoded in idiosyncratic cortical topographies. *elife* 9 (2020), e56601.
- [14] Kaiming He, Xiangyu Zhang, Shaoqing Ren, and Jian Sun. 2016. Deep residual learning for image recognition. In *Proceedings of the IEEE conference on computer vision and pattern recognition*. 770–778.
- [15] Tomoyasu Horikawa and Yukiyasu Kamitani. 2017. Generic decoding of seen and imagined objects using hierarchical visual features. *Nature communications* 8, 1 (2017), 15037.
- [16] Edward J Hu, Yelong Shen, Phillip Wallis, Zeyuan Allen-Zhu, Yuanzhi Li, Shean Wang, Lu Wang, and Weizhu Chen. 2021. Lora: Low-rank adaptation of large language models. *International Conference on Learning Representation*.
- [17] Xintao Hu, Fan Deng, Kaiming Li, Tuo Zhang, Hanbo Chen, Xi Jiang, Jinglei Lv, Dajiang Zhu, Carlos Faraco, Degang Zhang, Arsham Mesbah, Junwei Han, Xiansheng Hua, Li Xie, Stephen Miller, Lei Guo, and Tianming Liu. 2010. Bridging low-level features and high-level semantics via fMRI brain imaging for video classification. In *Proceedings of the 18th ACM International Conference on Multimedia*. 451–460.
- [18] Yukiyasu Kamitani and Frank Tong. 2005. Decoding the visual and subjective contents of the human brain. *Nature neuroscience* 8, 5 (2005), 679–685.
- [19] Dmitry Lepikhin, HyoukJoong Lee, Yuanzhong Xu, Dehao Chen, Orhan Firat, Yanping Huang, Maxim Krikun, Noam Shazeer, and Zhifeng Chen. 2021. GShard: Scaling Giant Models with Conditional Computation and Automatic Sharding. In *International Conference on Learning Representations*. OpenReview.net.
- [20] Sikun Lin, Thomas Sprague, and Ambuj K Singh. 2022. Mind reader: Reconstructing complex images from brain activities. *Advances in Neural Information Processing Systems* 35 (2022), 29624–29636.
- [21] Tsung-Yi Lin, Michael Maire, Serge J. Belongie, James Hays, Pietro Perona, Deva Ramanan, Piotr Dollár, and C. Lawrence Zitnick. 2014. Microsoft COCO: Common Objects in Context. In *European Conference on Computer Vision*, Vol. 8693. 740–755.
- [22] David Linden. 2021. Section 3 - Introduction. In *fMRI Neurofeedback*, Michelle Hampson (Ed.). Academic Press, 161–169. <https://doi.org/10.1016/B978-0-12-822421-2.00008-9>
- [23] Yulong Liu, Yongqiang Ma, Wei Zhou, Guibo Zhu, and Nanning Zheng. 2023. BrainCLIP: Bridging Brain and Visual-Linguistic Representation via CLIP for Generic Natural Visual Stimulus Decoding from fMRI. *arXiv preprint arXiv:2302.12971* (2023).
- [24] Ilya Loshchilov and Frank Hutter. 2017. Decoupled weight decay regularization. *International Conference on Learning Representation*.
- [25] Yizhuo Lu, Changde Du, Qiongyi Zhou, Dianpeng Wang, and Huiguang He. 2023. MindDiffuser: Controlled Image Reconstruction from Human Brain Activity with Semantic and Structural Diffusion. In *Proceedings of the 31st ACM International Conference on Multimedia*. 5899–5908.
- [26] Thomas Naselaris, Kendrick N Kay, Shinji Nishimoto, and Jack L Gallant. 2011. Encoding and decoding in fMRI. *Neuroimage* 56, 2 (2011), 400–410.
- [27] Xixi Nie, Bo Hu, Xinbo Gao, Leida Li, Xiaodan Zhang, and Bin Xiao. 2023. BMI-Net: A Brain-inspired Multimodal Interaction Network for Image Aesthetic Assessment. In *Proceedings of the 31st ACM International Conference on Multimedia*. 5514–5522.
- [28] Furkan Ozelcik and Rufin VanRullen. 2023. Brain-diffuser: Natural scene reconstruction from fmri signals using generative latent diffusion. *arXiv preprint arXiv:2303.05334* (2023).
- [29] Simone Palazzo, Concetto Spampinato, Isaak Kavasidis, Daniela Giordano, Joseph Schmidt, and Mubarak Shah. 2020. Decoding brain representations by multimodal learning of neural activity and visual features. *IEEE Transactions on Pattern Analysis and Machine Intelligence* 43, 11 (2020), 3833–3849.
- [30] Nikhil Parthasarathy, Eleanor Batty, William Falcon, Thomas Rutten, Mohit Rajpal, E. J. Chichilnisky, and Liam Paninski. 2017. Neural Networks for Efficient Bayesian Decoding of Natural Images from Retinal Neurons. In *Advances in Neural Information Processing Systems 30: Annual Conference on Neural Information Processing Systems*. 6434–6445.
- [31] Francisco Pereira, Bin Lou, Brianna Pritchett, Samuel Ritter, Samuel J Gershman, Nancy Kanwisher, Matthew Botvinick, and Evelina Fedorenko. 2018. Toward a universal decoder of linguistic meaning from brain activation. *Nature communications* 9, 1 (2018), 963.
- [32] Alec Radford, Jong Wook Kim, Chris Hallacy, Aditya Ramesh, Gabriel Goh, Sandhini Agarwal, Girish Sastry, Amanda Askell, Pamela Mishkin, Jack Clark, et al. 2021. Learning transferable visual models from natural language supervision. In *International conference on machine learning*. PMLR, 8748–8763.
- [33] Yongming Rao, Wenliang Zhao, Zheng Zhu, Jiwen Lu, and Jie Zhou. 2021. Global Filter Networks for Image Classification. In *Advances in Neural Information Processing Systems (NeurIPS)*.
- [34] Yongming Rao, Wenliang Zhao, Zheng Zhu, Jie Zhou, and Jiwen Lu. 2023. GFNet: Global Filter Networks for Visual Recognition. *IEEE Trans. Pattern Anal. Mach. Intell.* 45, 9 (2023), 10960–10973.
- [35] Carlos Riquelme, Joan Puigcerver, Basil Mustafa, Maxim Neumann, Rodolphe Jenatton, André Susano Pinto, Daniel Keysers, and Neil Houlsby. 2021. Scaling Vision with Sparse Mixture of Experts. In *Advances in Neural Information Processing Systems*. 8583–8595.
- [36] Pieter R Roelofsma, Damiaan Denys, and P Christiaan Klink. 2018. Mind reading and writing: the future of neurotechnology. *Trends in cognitive sciences* 22, 7 (2018), 598–610.
- [37] Paul S Scotti, Atmdeep Banerjee, Jimmie Goode, Stepan Shabalin, Alex Nguyen, Ethan Cohen, Aidan J Dempster, Nathalie Verlinde, Elad Yundler, David Weisberg, et al. 2023. Reconstructing the Mind’s Eye: fMRI-to-Image with Contrastive Learning and Diffusion Priors. *arXiv preprint arXiv:2305.18274* (2023).
- [38] Noam Shazeer, Azalia Mirhoseini, Krzysztof Maziarz, Andy Davis, Quoc V. Le, Geoffrey E. Hinton, and Jeff Dean. 2017. Outrageously Large Neural Networks: The Sparsely-Gated Mixture-of-Experts Layer. In *5th International Conference on Learning Representations*. OpenReview.net.
- [39] Guohua Shen, Tomoyasu Horikawa, Kei Majima, and Yukiyasu Kamitani. 2019. Deep image reconstruction from human brain activity. *PLoS computational biology* 15, 1 (2019), e1006633.
- [40] Yu Takagi and Shinji Nishimoto. 2023. High-resolution image reconstruction with latent diffusion models from human brain activity. In *Proceedings of the IEEE/CVF Conference on Computer Vision and Pattern Recognition*. 14453–14463.
- [41] Alexis Thual, Quang Huy Tran, Tatiana Zemska, Nicolas Courty, Rémi Flamary, Stanislas Dehaene, and Bertrand Thirion. 2022. Aligning individual brains with fused unbalanced Gromov Wasserstein. *Advances in neural information processing systems* 35 (2022), 21792–21804.
- [42] David C Van Essen, Stephen M Smith, Deanna M Barch, Timothy EJ Behrens, Essa Yacoub, Kamil Ugurbil, Wu-Minn HCP Consortium, et al. 2013. The WU-Minn human connectome project: an overview. *Neuroimage* 80 (2013), 62–79.
- [43] Ashish Vaswani, Noam Shazeer, Niki Parmar, Jakob Uszkoreit, Llion Jones, Aidan N Gomez, Łukasz Kaiser, and Illia Polosukhin. 2017. Attention is all you need. *Advances in neural information processing systems* 30 (2017).
- [44] Jun Wang, Eric Pohlmeier, Barbara Hanna, Yu-Gang Jiang, Paul Sajda, and Shih-Fu Chang. 2009. Brain state decoding for rapid image retrieval. In *Proceedings of*

- the 17th ACM International Conference on Multimedia*. 945–954.
- [45] Mengzhu Wang, Jianlong Yuan, and Zhibin Wang. 2023. Mixture-of-Experts Learner for Single Long-Tailed Domain Generalization. In *Proceedings of the 31st ACM International Conference on Multimedia*. 290–299.
 - [46] Wenhui Wang, Hangbo Bao, Li Dong, Johan Bjorck, Zhiliang Peng, Qiang Liu, Kriti Aggarwal, Owais Khan Mohammed, Saksham Singhal, Subhojit Som, and Furu Wei. 2023. Image as a foreign language: BEiT pretraining for vision and vision-language tasks. In *Proceedings of the IEEE/CVF Conference on Computer Vision and Pattern Recognition*.
 - [47] Yijun Zhang, Tong Bu, Jiyuan Zhang, Shiming Tang, Zhaofei Yu, Jian K Liu, and Tiejun Huang. 2022. Decoding pixel-level image features from two-photon calcium signals of macaque visual cortex. *Neural Computation* 34, 6 (2022), 1369–1397.
 - [48] Qiongyi Zhou, Changde Du, Shengpei Wang, and Huiguang He. 2024. CLIP-MUSED: CLIP-Guided Multi-Subject Visual Neural Information Semantic Decoding. (2024).
 - [49] Qianyu Zhou, Ke-Yue Zhang, Taiping Yao, Ran Yi, Shouhong Ding, and Lizhuang Ma. 2022. Adaptive Mixture of Experts Learning for Generalizable Face Anti-Spoofing. In *Proceedings of the 30th ACM International Conference on Multimedia*.

A DETAILS OF BACKBONE ARCHITECTURES

This section provides detailed statements for each backbone architecture used in our experiments.

A.1 MLP

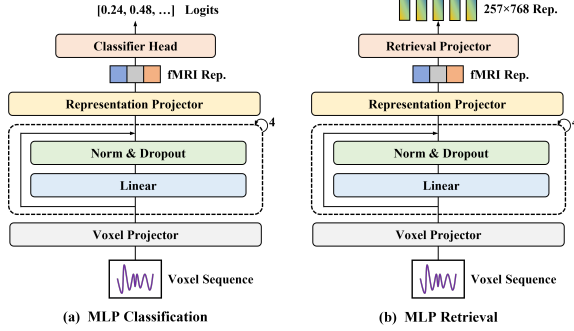


Figure 4: Architecture of MLP backbone. Figure (a) is designed for the classification task, and Figure (b) is designed for the cross-modal retrieval task.

The architecture of our MLP backbone, depicted in Figure 4, involves several key components. Initially, a **Voxel Projector** is employed to project the voxel sequence into a latent space of 4096 dimensions. This projector comprises a sequence of operations: a Linear layer, a LayerNorm, a GLUE activation function, and a Dropout. Following the above projection, the latent representations undergo further transformation within the latent space via 4 **Res-Blocks**. Each ResBlock includes a Linear layer, a LayerNorm, a GLUE activation, a Dropout, and a residual connection from input to output. For classification tasks, a Linear layer called **Representation Projector** projects the 4096-dimension latent representation into an fMRI representation of dimension 768. Subsequently, a **Classifier Head**, another Linear layer, produces logits for classification. In the case of retrieval tasks, the fMRI representation is structured as 257×768 . To enhance the representation, we employ a **Retrieval Projector** that extends its last dimension to 2048 before reducing it back to 768. This Retrieval Projector consists of three Linear layers, sequentially expanding (768 to 2048), maintaining (2048 to 2048), and then compressing (2048 to 768) the dimensionality. GLUE activations and LayerNorm operations are followed by each Linear layer throughout this process.

A.2 Transformer

Figure 5 illustrates the architecture of our Transformer backbone, employing the standard Vision Transformer (ViT) model¹. The Voxel Tokens and the CLS token undergo processing through 6 Transformer blocks. Each block comprises an 8-head Self-Attention layer alongside a FeedForward Network (FFN). Within the FFN, a layerNorm operation is initially applied, followed by an extension of the 768-dimensional tokens to 1024, subsequently reducing them back to 768 dimensions. In the classification task, the CLS token

¹GitHub repository: <https://github.com/lucidrains/vit-pytorch>

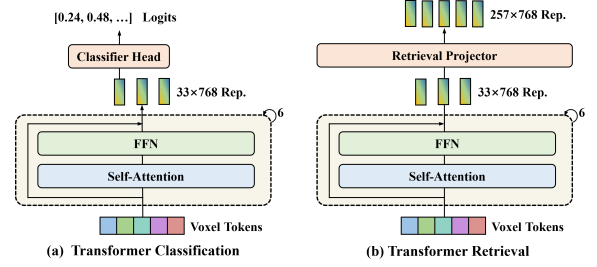


Figure 5: Architecture of Transformer backbone. Figure (a) is designed for the classification task, and Figure (b) is designed for the cross-modal retrieval task.

is directed to the Classifier Head, where it yields logits. For the retrieval task, we employ a Linear layer to expand the dimensionality of each non-CLS token to 8 times its original size, after which it's split into 8 tokens. This process results in a representation of size 257×768 .

A.3 GFNet

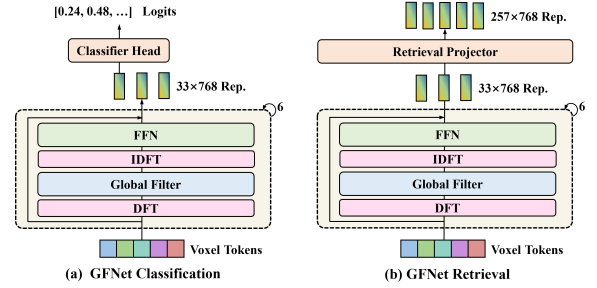


Figure 6: Architecture of GFNet backbone. Figure (a) is designed for the classification task, and Figure (b) is designed for the cross-modal retrieval task.

Figure 6 illustrates the architecture of our GFNet backbone. For the voxel tokens $T = T_0, T_1, T_2, \dots, T_n$, GFNet fuses them in the frequency domain. Specifically, it first employs a Discrete Fourier Transform (DFT) to obtain the spectrum of the voxel tokens:

$$F(k) = \sum_{j=0}^n T_j e^{-2k(\frac{2\pi}{n+1})i} \quad (14)$$

where i denotes the imaginary unit and $F(k)$ denotes spectrum at the frequency $\frac{2\pi}{n+1}k$. Subsequently, the spectrum is filtered with a filter $S \in \mathbb{C}^{(n+1) \times d}$:

$$F' = [F'(0), F'(1), \dots, F'(k)] = S \cdot [F(0), F(1), \dots, F(k)] \quad (15)$$

Finally, the voxel tokens can be recovered by the Inverse Discrete Fourier Transform (IDFT):

$$T'_j = \frac{1}{n+1} \sum_{k=0}^n F(k) e^{2j(\frac{2\pi}{n+1})i} \quad (16)$$

After frequency domain filtering, the voxel tokens are processed through a FeedForward Network, akin to a Transformer. We utilize 6 GFNet blocks to embed 33×768 fMRI representations. Subsequently,

Subject ID	Model Architecture	# of Parameters	mAP \uparrow	AUC \uparrow	Hamming \downarrow
Subj01	MLP	231M	0.476024	0.949119	0.022501
	Transformer	19M	0.427904	0.940943	0.023422
	GFNet	17M	0.464277	0.944939	0.023371
Subj02	MLP	231M	0.437036	0.942302	0.023604
	Transformer	19M	0.401251	0.932202	0.025042
	GFNet	17M	0.422089	0.938486	0.024911
Subj05	MLP	231M	0.506511	0.954630	0.022149
	Transformer	19M	0.479843	0.948485	0.023545
	GFNet	17M	0.477757	0.950345	0.023489
Subj07	MLP	231M	0.448364	0.933091	0.023876
	Transformer	19M	0.387984	0.924591	0.024669
	GFNet	17M	0.406180	0.931569	0.025123

Table 8: Classification results of our Wills Aligner on Subjects 1, 2, 5, and 7. All results are averaged over three runs.

Subject ID	Model Architecture	# of Parameters	Retrieval Accuracy	
			Image (fwd) \uparrow	Brain (bwd) \uparrow
Subj01	MLP	523M	95.353%	83.903%
	Transformer	38M	96.658%	86.064%
	GFNet	36M	95.264%	81.531%
Subj02	MLP	523M	95.098%	84.067%
	Transformer	38M	95.212%	81.625%
	GFNet	36M	95.014%	80.346%
Subj05	MLP	523M	83.940%	68.836%
	Transformer	38M	84.438%	66.344%
	GFNet	36M	89.972%	67.186%
Subj07	MLP	523M	84.354%	71.115%
	Transformer	38M	84.656%	66.344%
	GFNet	36M	85.990%	68.699%

Table 9: Retrieval results of our Wills Aligner on Subjects 1, 2, 5, and 7. All results are averaged over three runs. All the models adopt CLIP loss as the supervise objective.

we employ the identical Classifier Head and Retrieval Projector for both classification and retrieval tasks.

B ADDITIONAL EXPERIMENTAL RESULTS

B.1 Detailed Classification Results

In order to facilitate subsequent work to develop comparisons, we provide the classification results of our wills aligner on subjects 1, 2, 5, and 7, respectively. As shown in Table 8, we observe that the classification accuracy of Subj01 and Subj05 is higher than the average level, while that of Subj02 and Subj07 is lower than the average level. The non-negligible differences in classification accuracy between subjects may be attributed to the inherent signal-to-noise ratio of the subjects’ fMRI data. We also observe that the performance ranking of the three backbone architectures appears consistent across different subjects.

B.2 Detailed Retrieval Results

We provide the retrieval results of our wills aligner on subjects 1, 2, 5, and 7 in Table 9. We found significant differences between Subj01,

Subj02, and Subj05, Subj07, where the former exhibit a forward retrieval accuracy of up to 95%, while the latter can only achieve 85%. The observed disparity doesn’t align with our findings in the classification task. We attribute this phenomenon to two factors. On the one hand, the differing demands between classification and retrieval tasks, specifically the need for coarse-grained visual information versus fine-grained visual information. Due to potential variations in subjects’ attentional focus and cognition patterns, the number of different granularity levels of visual information within the same fMRI data varies. On the other hand, differences in model architectures may also contribute to this phenomenon. The use of a retrieval projector instead of a classification head in our retrieval task’s model architecture leads to distinct representation learning capabilities, and thus, the representations learned are different.

B.3 Additional Few-shot Results

Tables 10 and Table 11 show the performance of the Transformer architecture versus the GFnet architecture for different few-shot ratios, respectively. We observe that different backbone networks perform similarly for the same few-shot ratio. This suggests that the

Backbone	Few-Shot Ratio	Subject 1		Subject 2		Subject 5		Subject 7	
		mAP ↑	AUC ↑						
Transformer	0.05	0.267	0.899	0.229	0.881	0.272	0.904	0.204	0.857
	0.1	0.306	0.915	0.286	0.898	0.324	0.919	0.261	0.886
	0.2	0.368	0.926	0.323	0.918	0.383	0.935	0.315	0.905
GFNet	0.05	0.262	0.900	0.235	0.884	0.277	0.911	0.215	0.868
	0.1	0.318	0.918	0.290	0.904	0.329	0.921	0.275	0.888
	0.2	0.376	0.928	0.341	0.920	0.396	0.936	0.323	0.909

Table 10: More results of few-shot classification.

Backbone	Few-Shot Ratio	Subject 1		Subject 2		Subject 5		Subject 7	
		Image ↑	Brain ↑						
Transformer	0.05	64.4%	47.4%	69.9%	49.9%	47.2%	29.6%	45.2%	28.4%
	0.1	76.1%	53.4%	75.7%	56.0%	54.4%	35.9%	54.3%	39.1%
	0.2	83.7%	59.6%	83.8%	64.0%	63.8%	45.1%	62.9%	46.1%
GFNet	0.05	65.2%	48.4%	71.2%	50.8%	46.6%	28.3%	45.9%	29.8%
	0.1	75.3%	52.4%	77.7%	56.6%	53.9%	35.0%	54.8%	38.7%
	0.2	83.1%	60.2%	85.4%	63.8%	63.7%	44.6%	63.2%	47.9%

Table 11: More results of few-shot retrieval.

Backbone	Rank	Classification			Retrieval	
		mAP ↑	AUC ↑	Hamming ↓	Brain (fwd) ↑	Image (bwd) ↑
Transformer	2	0.442	0.942	0.024	94.0%	82.6%
	4	0.438	0.942	0.024	93.9%	82.8%
	8	0.448	0.943	0.024	95.1%	84.1%
	16	0.424	0.937	0.024	96.6%	86.1%
	32	0.450	0.943	0.024	95.0%	84.3%
GFNet	2	0.447	0.943	0.025	93.0%	80.1%
	4	0.450	0.943	0.024	94.6%	83.4%
	8	0.447	0.945	0.024	94.4%	82.4%
	16	0.443	0.945	0.023	95.3%	81.5%
	32	0.451	0.944	0.024	94.7%	84.0%

Table 12: More ablation experiments for rank. Consistent with the main text, for the classification task, we report the average value over four subjects; for the retrieval task, we only show the retrieval accuracy for subject 1.

choice of different backbones does not lead to substantial changes in performance, demonstrating that our Wills Aligner is robust.

B.4 Additional Ablation

Table 12 displays the performance of the Transformer architecture versus the GFNet architecture under different ranks. We can re-verify from this the conclusion in the main text that Wills Aligner is not sensitive to the selection of rank in MoBE. This suggests that there is no need for a hyperparametric search for rank when our method is applied to other tasks. Specifically, we can simply set the rank to 8 or 16. Furthermore, since we can use a MoBE with a smaller rank while not losing too much precision, our method can

be extended to datasets with a large number of cognition patterns without introducing too much extra parameter overhead.

C ADDITIONAL VISUALIZATION

C.1 Additional Correct Retrieval Visualization

We show more correct retrieval cases of each subject, as shown in Figure 7. The backbone architecture employed for visualization is the Transformer. Its forward retrieval accuracy is at 96.7%, 95.2%, 84.4%, and 84.7% across four distinct subjects. We observe that correctly retrieved images tend to be semantically simple and clear images with a single background color and content. The visual

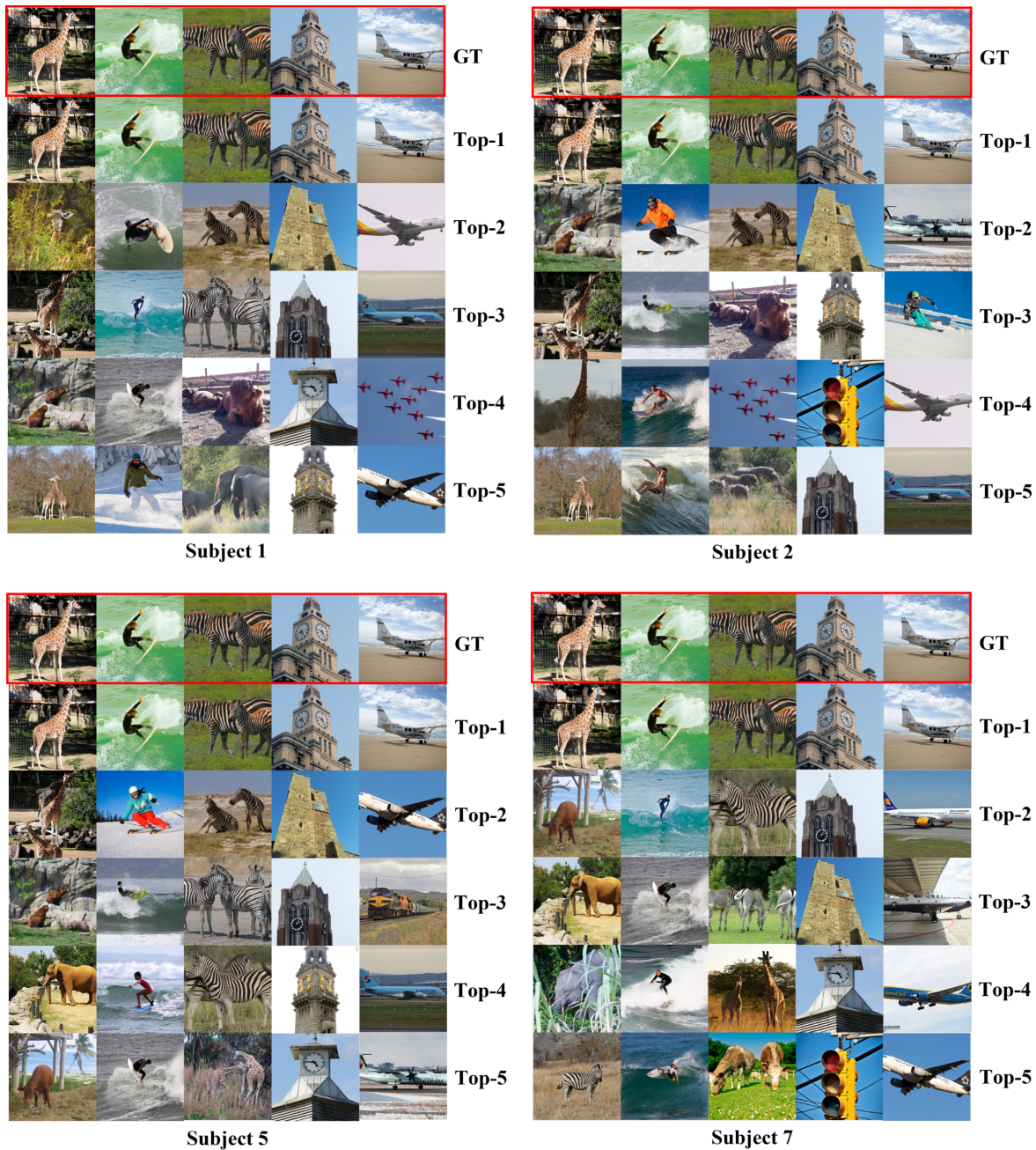


Figure 7: Additional correct retrieval examples. GT denotes the seen images by each subject.

stimuli generated by seeing these images are easy to derive fine-grained visual information from. We also find that even with a 10% gap in top-1 retrieval accuracy, the top 2-5 retrieval results for subjects 5 and 7 are almost always semantically relevant images, indicating that the model trained by our Wills Aligner is able to decode the visual information in fMRI adequately. Of course, we also observe that some semantically very similar but different incorrect retrieval results appear in the top 2-5 retrieval results.

C.2 Additional Incorrect Retrieval Visualization

As shown in Figure 8, we show some cases of incorrect retrieval for Subject 1. We observe that incorrect retrieval images tend to be for semantically rich images with complex scenes. Due to their extreme complexity, it is also difficult for the brain's visual cortex to extract the complete semantics accurately, thus making the fMRI lose some detailed information, leading to erroneous results. In addition, the proportion of semantically irrelevant images becomes higher in the top2-5 retrieval results, which we believe is also related to the

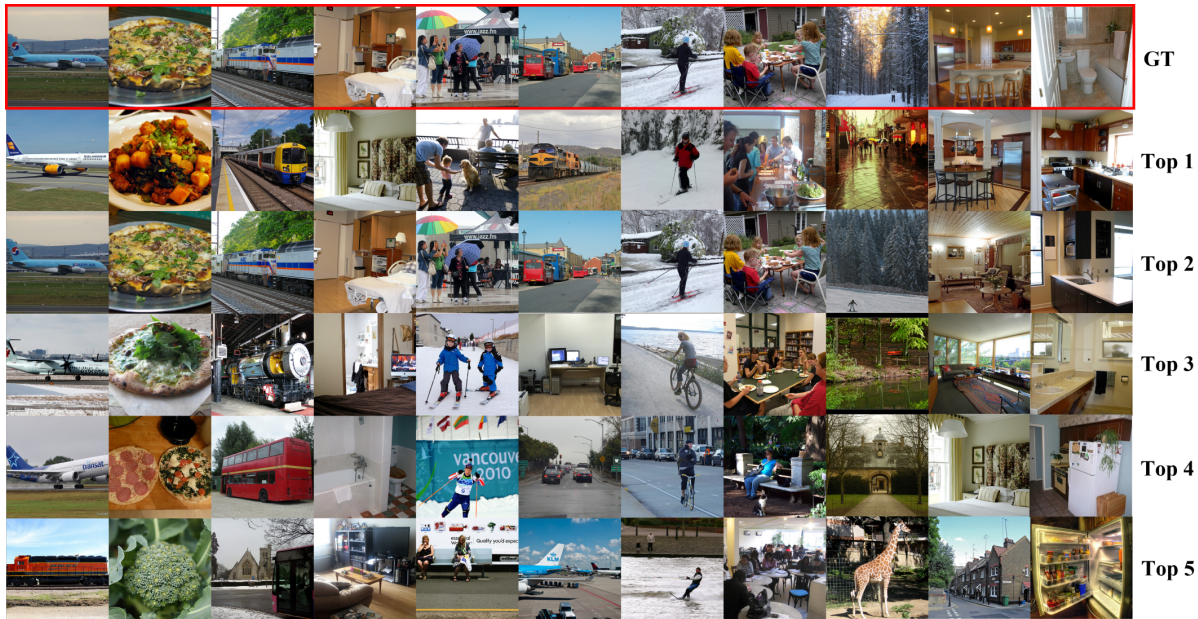


Figure 8: Additional incorrect retrieval examples. GT denotes the seen images by each subject. These 11 images are divided into two categories: the GTs of the first 8 images appear in the top-2 positions, which account for the majority of the incorrect retrieval examples, while the GTs of the last 3 images do not appear in the top-5 retrieval results, which account for a very small number of cases.

retrieval pool. In the NSD test set of 982 samples, images featuring zebras, trains, giraffes, surfing, skiing, architecture, airplanes, and the like are more prevalent, while those depicting food, crowds, furniture, etc., are less common. This decreases semantic relevance for the top 2-5 retrieval results of the latter.

D MORE DISCUSSION

D.1 Regarding Visual Reconstruction

In our study, we performed two types of tasks, visual classification, and cross-modal retrieval, without visual reconstruction as in some of the papers. This is due to the fact that almost all existing visual reconstructions are based on retrieval. They usually perform a retrieval task to obtain an fMRI representation similar to the picture

representation and utilize pre-trained, fixed generative models (e.g., Stable Diffusion, Versatile Diffusion, etc.) to achieve visual reconstruction. Essentially, this visual reconstruction merely visualizes the visual semantics in the fMRI representation, which is not very different from the essence of the retrieval task, and thus, we chose the more essential retrieval task over the reconstruction task.

D.2 Regarding Image Representations

We note that image representation embedded by a larger CLIP ViT can yield better cross-modal retrieval accuracy, e.g., using the existing ViT-H/14 or ViT-bigG/14. However, for a fair comparison, we use the image representations embedded by ViT-L/14, which are consistent with previous work. We recommend using a larger ViT for better results in follow-up work and other applications.